High-spin study of the shell model nucleus ^{88}Y_{49}

M. Bunce, P. H. Regan, V. Werner, C. W. Beausang, V. Anagnostatou, M. Bowry, R. J. Casperson, D. Chen, N. Cooper, P. M. Goddard, R. O. Hughes, G. Ilie, P. J. R. Mason, B. Pauerstein, M. W. Reed, T. J. Ross, and E. C. Simpson

Phys. Rev. C **87**, 044337 — Published 30 April 2013

DOI: 10.1103/PhysRevC.87.044337

High-Spin Study of the Shell Model Nucleus $^{88}\mathbf{Y}_{49}$

M. Bunce,[1,*] P.H. Regan,[1] V. Werner,[2] C.W Beausang,[3] V. Anagnostatou,[1] M. Bowry,[1] R.J. Casperson,[4] D. Chen,[3] N. Cooper,[2] P.M. Goddard,[1] R.O. Hughes,[3] G. Ilie,[2,5] P.J.R. Mason,[1] B.Pauerstein,[3] M.W. Reed,[1,6] T.J. Ross,[1,3] and E.C. Simpson[1]

[1]*Department of Physics, University of Surrey, Guildford, GU2 7XH, UK*

[2]*Wright Nuclear Structure Laboratory, Yale University, New Haven, Connecticut 06520-8120, USA*

[3]*Department of Physics, University of Richmond, Richmond, Virginia 23173, USA*

[4]*Lawrence Livermore National Laboratory, Livermore, CA 94551, USA*

[5]*National Institute for Physics and Nuclear Engineering, R-77125, Bucharest-Magurele, Romania*

[6]*Department of Nuclear Physics, R.S.P.E, Australian National University, Canberra, ACT 0200, Australia*

(Dated: January 30, 2013)

Abstract

The near-yrast structure of the near-magic, odd-odd nucleus, $^{88}_{39}Y_{49}$, has been studied into the high-spin regime. Investigations were performed at the Wright Nuclear Structure Laboratory, Yale University, using the ^{74}Ge(^{18}O,p3n) and ^{76}Ge(^{18}O,p5n) fusion-evaporation reactions at beam energies of 60 MeV and 90 MeV respectively. Gamma-ray energy coincidence analysis using both double (γ^2) and triple (γ^3) fold coincidences, together with angular correlation measurements have been used to extend the previously reported level scheme to an excitation energy of 8.6 MeV and spin/parity of $19^{(-)}$. The presented level scheme is compared with predictions of a truncated valence space shell model calculation, which assumes an inert ^{56}Ni core with proton and neutron excitations allowed within the $f_{5/2}$, $p_{3/2}$, $p_{1/2}$ and $g_{9/2}$ single particle states. The shell model calculations show a reasonable comparison with the experimental data for the yrast, positive-parity states up to spin 18 $\hbar$, with larger variations evident for negative parity states with spins greater than 16 $\hbar$. In spite of a significant increase in angular momentum input associated with the thin target ^{76}Ge(^{18}O,p5n) reaction channel, as compared to the backed target data using the ^{74}Ge target, no additional discrete states were identified in the former data set, suggesting that the level scheme for this nucleus fragments significantly above the observed states, possibly indicating cross-shell excitations becoming dominant for $I > 19$ $\hbar$.

PACS numbers: 23.20.-g, 23.20.Lv, 21.60.Cs and 27.50.+e

*Corresponding author: m.bunce@surrey.ac.uk

I. INTRODUCTION

The nucleus ^{88}Y, has a single neutron hole in the N=50 shell and a single proton hole in the sub-shell at Z=40. This proximity to magic and semi-magic numbers suggests that the low-lying excitations for this nucleus are likely to be characterised by simple single particle configurations that can be well described by the spherical-basis shell model. A number of previous studies have been carried out on the structure of ^{88}Y in the low spin regime [1–5], however, there are few investigations of the high spin states [6]. The maximum spin that can be generated from the particles in the valence space covering the $f_{5/2}$, $p_{3/2}$, $p_{1/2}$ and $g_{9/2}$ orbitals for ^{88}Y is 24 $\hbar$, with higher spin states requiring excitations across the ^{100}Sn core. A recent publication by Xu *et al.* [7] reported high spin states of ^{88}Y populated following the heavy-ion fusion evaporation reaction ^{82}Se(^{11}B, 5n)^{88}Y. The level scheme for ^{88}Y presented in the current work is compared with that reported by Xu *et al.,* and to the predictions of truncated basis shell model calculations assuming excitations between the closed ^{56}Ni and ^{100}Sn doubly magic cores.

II. EXPERIMENTAL DETAILS

Heavy-ion fusion-evaporation reactions were used to produce ^{88}Y to allow the investigation of the near-yrast states up to spins of $\sim$20 $\hbar$. The 21 MV ESTU Tandem Van de Graaff accelerator at the Wright Nuclear Structure Laboratory, Yale University, produced a beam of ^{18}O which was used to create the nucleus of interest via the reactions ^{74}Ge(^{18}O,p3n)^{88}Y and ^{76}Ge(^{18}O,p5n)^{88}Y. In the first experiment, a beam of ^{18}O at a laboratory energy of 60 MeV impinged a 600 μg/cm^2 ^{74}Ge target with a thick (10 mg/cm^2) ^{197}Au backing. The second experiment, aimed at accessing higher spins, used a higher beam energy (90 MeV) on a thin ^{76}Ge target (62 μg/cm^2 on a 20 μg/cm^2 carbon backing). Fusion evaporation cross-section calculations were performed using `PACE4` [8, 9] to estimate the optimum beam energies for the reactions used. These calculations estimated the semi-classical maximum angular momentum input into the compound nuclei for these two reactions to be $\sim$23 $\hbar$ and $\sim$40 $\hbar$ respectively.

Discrete energy gamma rays emitted following these reactions were measured using the YRAST ball germanium detector array [10]. In the current work, the array comprised

10 Compton suppressed (BGO shielded) HPGe clover detectors centred around the target chamber at a typical target-detector distance of 20 cm. The array was arranged to allow γ-ray coincidence angular correlations measurements with 6 clover detectors at an angle of θ=90° to the beam axis and 4 clover detectors at θ=42.5° (two upstream and two downstream relative to the target chamber).

The hardware logic trigger for the data acquisition system was set to accept mutually coincident, independent Compton suppressed events in at least three of the ten clover detectors within a 500 ns electronic hardware time logic window. A 'triples' clover coincidence (γ^3) master trigger was chosen to reduce system dead time and improve the overall coincidence spectral quality by ensuring that the accepted events arose from gamma-ray cascades with at least three discrete members. The data were sorted offline using the sort code `CSCAN` [11]. Table I provides a summary of the experimental details and number of events for each experiment in the current work.

TABLE I: Experimental details.

Beam	E_B (MeV)	Target	Backing	Beam current (pnA)	Master trigger rate	γ^3 events
^{18}O	60	^{74}Ge	^{197}Au	∼2	∼3 kHz	3.08x10^9
^{18}O	90	^{76}Ge	^{12}C	∼8	∼2 kHz	2.15x10^9

III. RESULTS

Events corresponding to gamma rays emitted from the decay of excited nuclear states in ^{88}Y were sorted off-line into 2-D (γ^2) matrices and 3-D (γ^3) coincidence cubes for investigation using the `RADWARE` analysis suite [12]. Figure 1 shows the total projections of the γ^2 matrices constructed from the 'backed target' and 'thin target' data in the current work. Previously reported gamma rays identified as originating from ^{88,89}Y and ^{88,89}Zr [13, 14] are marked. The most intense of these are associated with transitions from the 4n evaporation channel, ^{88}Zr [14].

The level scheme for ^{88}Y deduced in the current work is shown in Figure 2 (intensities correspond to the backed target data). Coincident timing analysis techniques were used to remove random coincident events. The timing analysis involved setting various software gating conditions on time differences between measured gamma rays relative to the master trigger. A software time difference coincidence condition of $\pm$90 ns was applied to the γ^2 matrices as it provided the optimum compromise between removal of random gamma rays and reduction in overall statistics.

The investigation of gamma-ray coincidence relationships allows for the confirmation of previously published level schemes. Figure 3 shows projections of γ^2 matrices for the backed and thin target data sets gated on the 312 keV I^{π}=12$^-$ $\rightarrow$ 11$^-$ transition in ^{88}Y. Figure 4 shows the projections of the symmetrised γ^3 coincidence cube with gates on the 214 and 312 keV transitions associated with ^{88}Y, for the backed and thin target data. Notably, the relative intensity of the high lying excitations is increased in the thin target (higher spin-input) data as expected, however, no additional discrete energy transitions were identified in the thin target data set.

The Directional Correlation of Oriented states (DCO) method was used to determine the likely angular momentum carried by the observed gamma rays. A $\gamma(90^{\circ})$-$\gamma(42.5^{\circ})$ coincidence matrix was constructed such that the axes corresponded to the two angular groups of detectors within the YRAST ball array. A gate with an energy corresponding to a previously reported transition of a well defined multipolarity was then applied to both axes of this matrix. A ratio of the intensity of the projected gamma ray peaks was measured, allowing coincident transitions with different multipolarities to be differentiated. The results of the DCO analysis of the backed and thin target data for ^{88}Y from the current work are summarised in Table II.

The current work confirms the results published by Warburton *et al.* [6] and extends the level scheme from 15$\hbar$ to 19$\hbar$, identifying 10 additional transitions in the high spin regime. A recent study by Xu *et al.* [7] reports many of same transitions but with a different placement to the current work. The current work places the 1608 keV transition decaying from the E_x=2312 keV I^{π}=9$^+$ level, populating the E_x=705 keV spin 7 level. This energy is consistent with a level assigned with I^{π}=(7$^+$) following light-ion transfer reactions in ref. [16]. Such a state would be expected to be isomeric in nature. Xu *et al.* [7] assigned the 1608 keV transition to populate the 5558 keV level with tentative spin/parity I^{π}=16$^-$. Evidence for

the revision of the placement of this transition in the current work is shown in Figures 6 and 7. Panels (a)-(e) in Figure 6 (backed target data) show projections of double gated γ^3 coincidence data with the gates set on the 5 highest lying transitions in the main cascade (734, 435, 544, 575 and 307 keV) as shown in Figure 2. The absence of a discrete peak at 1608 keV indicates that this energy is not mutually coincident with these gamma rays. The same conclusion is reached after analysis of the thin target data. Figure 7 shows projections of double gated γ^3 data (backed target) with the gates set on the 1608 keV and a sum of 312 and 214 keV, 1208 keV and 1769 keV respectively. Panel (a) shows the 1608 keV γ-ray to be coincident with 395 keV and 944 keV, but not with 1638 keV and 1769 keV, leading to the conclusion that the 1608 keV de-populates the E_x=2312 keV $I^\pi=9^+$ level. Further support for this placement is the appearance of the weak 131 keV transition in this gate, as well as the 1208 keV peak. Panel (b) provides the same conclusion, with the 131, 214, 312, 646 and 734 keV transitions (but not 395 and 944 keV) present in panel (a). Panel (c) shows no peaks that correspond to previously reported gamma rays assigned to ^{88}Y, indicating that 1608 keV is not coincident with the 1769 keV transition. The data presented in this work also indicates that the γ ray de-exciting the 4178 keV level (214 keV) has multipolarity ΔI=1 (see Table II), which is consistent with the study of Warburton *et al.* [6]. This is contrary to the results published in [7] which assigns this transition ΔI=2. As a result of this discrepancy, the tentatively assigned positive parity side branch shown in Figure 2 is consistent with the branch labeled 'C' in Xu *et al.* [7] but with the member levels spins reduced by 1 $\hbar$.

Two tentatively placed levels for ^{88}Y in the current work are at excitation energies of 9142 and 9614 keV. The two gamma rays depopulating these levels are seen in the inset plots of Figures 3 and 4. Projections of the energy gates placed on these transitions in the γ^3 coincidence cube with second gates placed on the 214, 312 and 646 keV transitions are shown in Figure 8. Panel (a) shows the 2033 keV gate with the 214, 312, 396, 435, 546, 575, 646, 734, 1208, 1760 keV gamma rays present but not the 307 keV transition. This indicates the 2033 keV transition feeds directly into the level scheme at the E_x=7109 keV level. Panel (b) shows the projection of the 3081 keV gate with the 214, 312, 396, 435, 546, 646, 734, 1208, 1769 keV transitions present. The 575 and 307 keV transitions are not present in this projection suggesting the 3081 keV gamma ray populates the E_x=6533 keV level. The parities of the previously unreported levels are assigned tentatively on the basis

of comparison with the shell model calculations discussed in the next section.

IV. SHELL MODEL CALCULATIONS AND DISCUSSION

Truncated basis shell model calculations were carried out for ^{88}Y using the code NuShellX [15]. The valence space used covered the major shell from Z, N=28-50, with a ^{56}Ni inert core. No sub-shell truncations were applied to this model space, allowing the valence particles to move freely between the $f_{5/2}$, $p_{3/2}$, $p_{1/2}$ and $g_{9/2}$ single particle orbitals. The interaction chosen was based on the Bonn-C potential, with the four single particle energies, $f_{5/2}$(-8.7087 MeV), $p_{3/2}$(-9.8280 MeV), $p_{1/2}$(-7.8388 MeV) and $g_{9/2}$(-6.2617 MeV), modified empirically to fit experimental energy data in the region A=63-96, including ^{89}Y, see ref. [16]. The highest spin/parity configurations possible for the valence space used in the current work are 23^- and 24^+ (see Table III).

^{88}Y has one neutron hole in the N=28-50 major shell. The calculations have no sub-shell restrictions on the neutrons, however, it is clear from the results of these calculations that the $\nu(g_{9/2})^{-1}$ is the only neutron configuration of significance. There are also no sub-shell restrictions placed upon the proton single particle orbitals, allowing free movement of the 11 valence protons in the 'fpg' major shell. The results of the shell model calculations are shown in Figure 5, with detailed results presented in Table III. Figure 5 shows the experimental level scheme of ^{88}Y deduced in the current work alongside the shell model calculations for ^{88}Y. The calculations for ^{88}Y show reasonable agreement with the experimental yrast level schemes up to excitation energies of $\sim$5 MeV. These lower-spin and excitation yrast levels are well described by simple configurations. For example, the I^π=4^- and 5^- state wavefunctions in ^{88}Y consist of more than 80% $\pi(p_{1/2})$ $\nu(g_{9/2})$ with other particle configurations contributing less than 5% each to the wavefunction. The shell model calculation predicts the yrast I^π=8^+ state to have an excitation energy of 823 keV. The general agreement between theory and experiment holds well, with differences of less than 200 keV, for the negative parity states up to the I^π=15^-, E_x=5766 calculated state. Above this the difference between the theoretical and experimental results increases to more than 1 MeV, possibly suggesting competition from cross-core excitations in the formation of near-yrast states in this energy range.

As with the negative parity states, the predicted positive parity states show a reasonable

agreement with the experimental results at lower excitation energies, however, the agreement extends to higher energies of ∼8.6 MeV. Figure 2 shows that the predicted higher energy positive parity states are consistent with those states identified in a parallel side branch. If these side branch states had negative parity, i.e. the same parity of the main decay sequence, one would expect to observe competing E2 transitions from the E_x=6266 keV spin 14 state to the E_x=3964 keV I^π=12$^-$ state and from the E_x=6815 keV spin 15 state to the E_x=4178 keV I^π=13$^-$ state. The energy of such transitions would be 2302 keV and 2637 keV respectively but there is no evidence of such discrete energies in the current work, consistent with positive parity assignments for the side branch levels.

The shell model calculations predict that the yrast I^π=19$^+$ state should be ∼500 keV above the observed I^π=18$^+$ yrast state. No firm evidence for a state corresponding to this predicted level is observed in the current work. The yrast I^π=20$^+$ and 20$^-$ states are predicted to lie almost 3 MeV above the I^π=19$^+$ state (see Table III) which suggests an exhaustion of energetically favoured angular momentum couplings in this valence space. The large energy gap suggests that cross-shell excitations may compete with such transitions, fragmenting the potential population of states with $I \geq 20\hbar$.

It was expected that the heavy-ion fusion evaporation reactions would impart angular momentum up to 40 $\hbar$ to the nucleus under study. However, it can be seen in Figure 2 that the extended experimental level scheme for ^{88}Y, only exhibits levels up to a spin of 19 $\hbar$. It is possible that no discrete levels are observed at higher spins in the current work due to the level scheme fragmenting, with a large number of weakly populated levels that are difficult to observe discretely.

Above ∼5 MeV the agreement between experiment and theoretical prediction becomes weaker. At some stage, the excitation energy will become sufficient for a neutron excitation across the N=50 shell gap. The N=50 shell gap is of the order of several MeV meaning within the energy range being examined it is possible for neutrons to excite across the gap. However, the calculation model space used includes only single particle states up to $g_{9/2}$ for both protons and neutrons, therefore allowing no excitations across the N=50 shell gap. This is likely to be the source of the large differences between the shell model calculations and the experimental levels scheme at high excitation energies.

V. CONCLUSIONS

A spectroscopic study of the near magic, odd-odd, nucleus ^{88}Y has been performed. Previously unreported data has been used to present a level scheme that extends to higher excitation energy and spin than previously reported. Angular correlation measurements were performed allowing the confirmation of previously reported level angular momentum and newly observed level angular momentum to be assigned. Shell model calculations were performed using NuShellX and reasonable agreement between experimental data and theoretical predications was achieved for states with $I \leq 18\hbar$. No evidence for decays from discrete levels with $I \geq 20\hbar$ was observed in the current work, in spite of a semi-classical angular momentum of >40 $\hbar$ being imparted. This suggests a complex fragmentation of the level scheme for ^{88}Y above $I \geq 18\hbar$ associated with excitations across the N=50 closed shell.

VI. ACKNOWLEDGMENTS

The author would like to acknowledge the excellent work of all the technical staff at the Wright Nuclear Structure Laboratory. This work is supported by STFC UK, EP/D077133/1, and U.S. DOE under grant no. DE-FG02-91ER40609, DE-FG52-06NA26206 and DE-FG02-05ER41379.

[1] F. Gabbard, G. Chenevert and K. K. Sekharan, Phys. Rev. C **6** 2167 (1972)

[2] M. Davidson, J. Davidson and M. A. J. Mariscotti, Nuclear Physics A **352** 237 (1981)

[3] H. W. Baer *et al.*, Nuclear Physics A **218** 355 (1974)

[4] J. R. Comfort and J. P. Schiffer, Phys. Rev. C **4** 803 (1971)

[5] J. L. Horton and C. E. Hollandsworth, Phys. Rev. C **13** 2212 (1976)

[6] E. K. Warburton *et al.*, J. Phys. G **12** 1017 (1986)

[7] C. J. Xu *et al.*, Phys. Rev. C **86** 027302 (2012)

[8] O. B. Tarasov and D. Bazin, Nucl. Instum. and Meth. A **204**, 174 (2003)

[9] A. Gavron, Phys. Rev. C **21** 230 (1980)

[10] C. W. Beausang *et al.*, Nucl. Instr. and Meth. A. **452**, 431 (2000)

[11] M. A. Caprio and J. J. Ressler, `cscan` sorting package and site-specific routines (unpublished).

[12] D. C. Radford, Nucl. Instum. and Meth. A **361**, 297 (1995)

[13] G. Mukherjee and A. A. Sonzogni, Nuclear Data Sheets **105** 419 2005

[14] B. Singh, Nuclear Data Sheets **85** 1 1998

[15] B. A. Brown and W. D. M. Rae, Nushell@MSU MSU-NSCL report (2007)

[16] M. Honma, T. Otsuka, T. Mizusaki and M. Hjorth-Jensen, Phys. Rev. C **80** 064323 (2009)

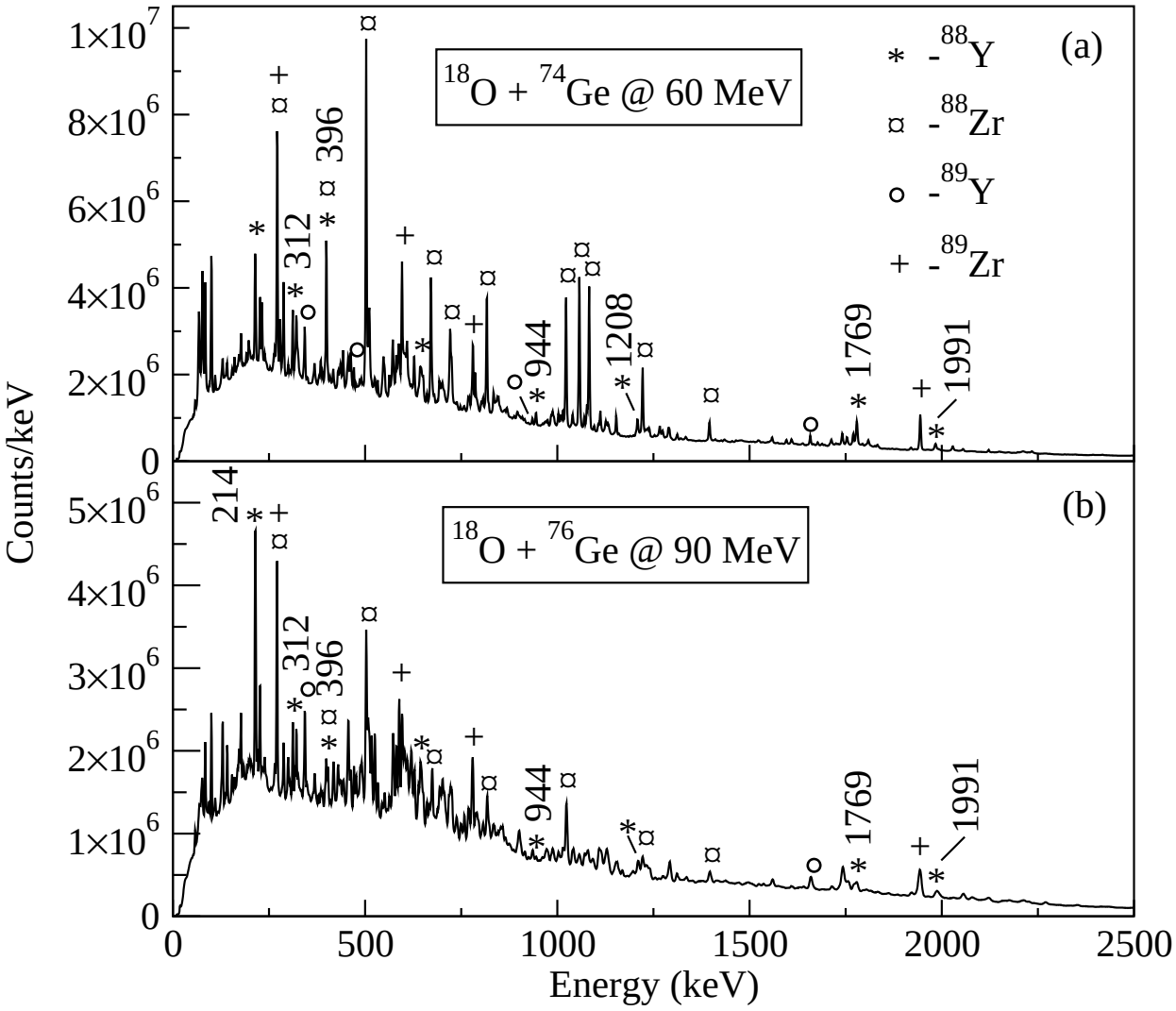

FIG. 1: Total projection of ungated symmetrised γ^2 matrices from the (a) backed target and (b) thin target experiments described in the current work.

-

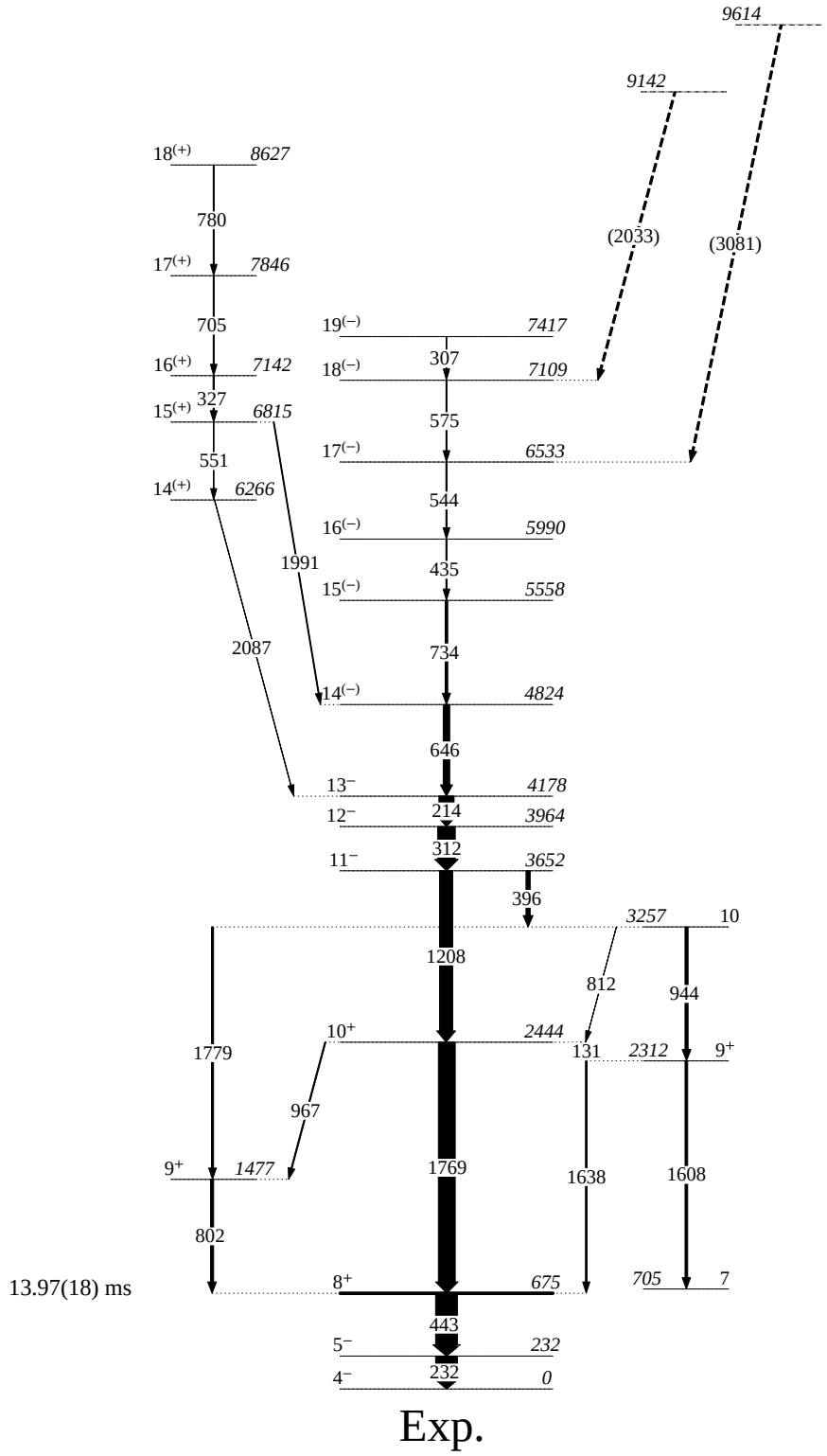

FIG. 2: Experimental level scheme for ^{88}Y constructed in the current work.

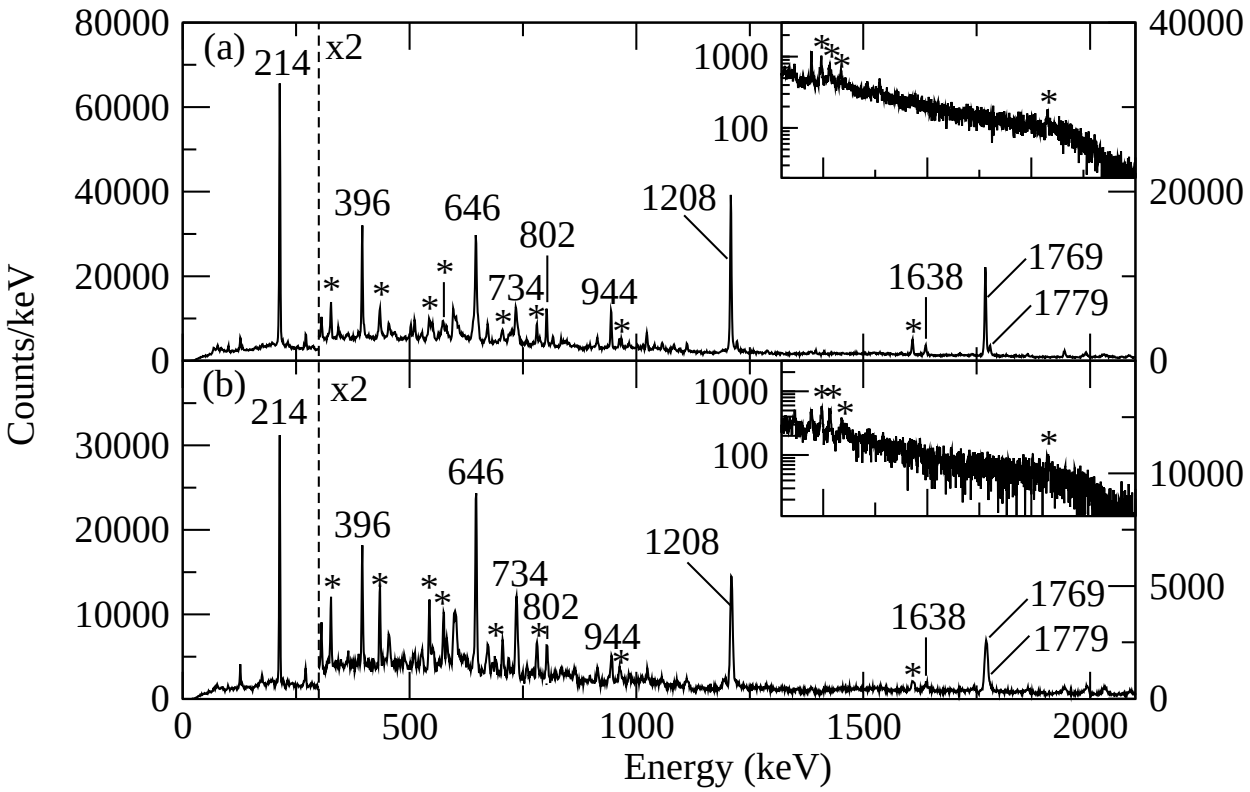

FIG. 3: Comparison of the (a) backed and (b) thin target γ^2 data with a gate set on the 312 keV transitions. Inset plots x-axis range from 1800-3500 keV. * indicates gamma-ray transitions associated with ^{88}Y in the current work but not reported by [6].

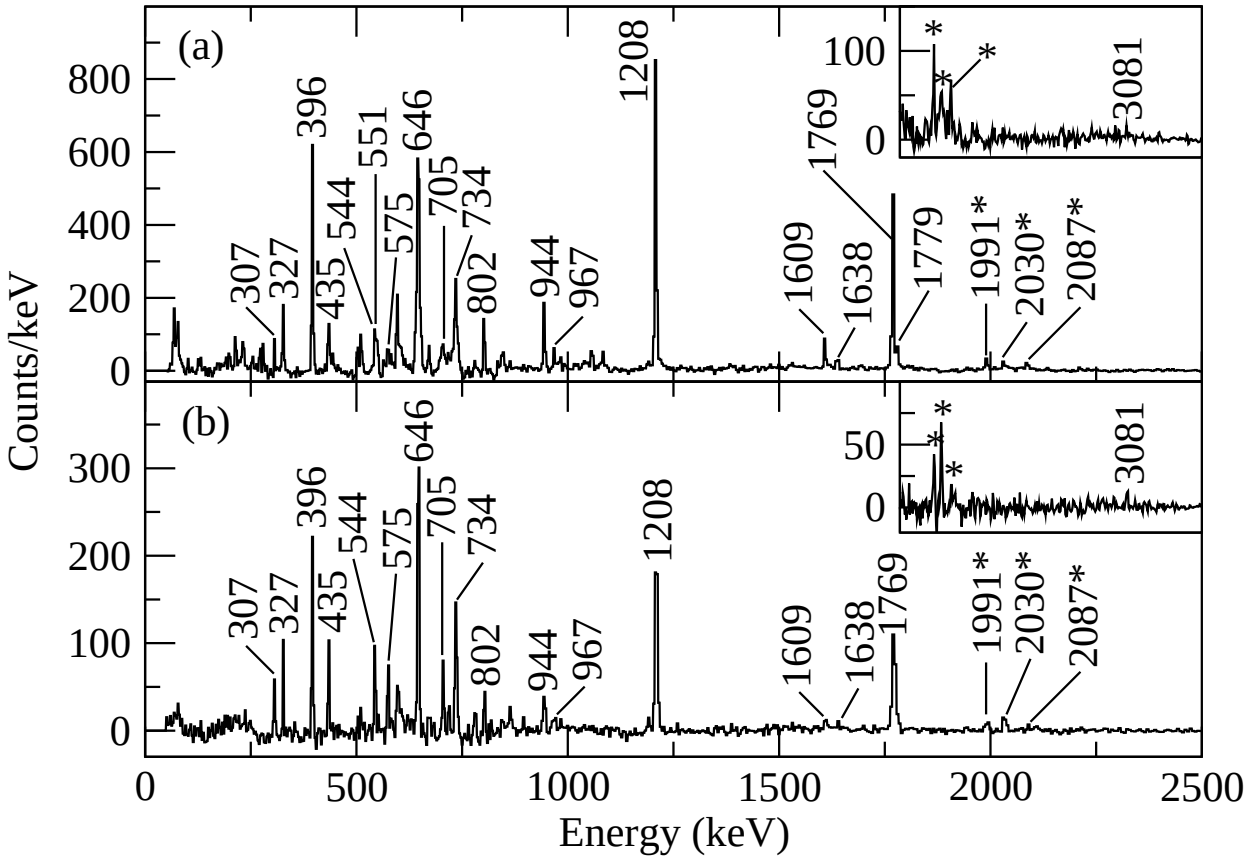

FIG. 4: Comparison of the (a) backed and (b) thin target γ^3 cube data with gates set on the 214 keV and 312 keV transitions. Inset plots x-axis range from 1800-3500 keV. Energies with * correspond to the three peaks in the inset plot.

TABLE II: Experimental Results for ^{88}Y

E_γ (keV)	$E_i \rightarrow E_f$ (keV)	$I_i^\pi \rightarrow I_f^\pi$ ($\hbar$)	$I_{rel}^{60\ MeV}$	$I_{rel}^{90\ MeV}$	$R_{DCO}^{60\ MeV}$		$R_{DCO}^{90\ MeV}$	
					1769(E2)	1208(E1)	1769(E2)	1208(E1)
131.4(10)	2444→2312	$10^+ \rightarrow 9^+$	2.7(5)	3.9(15)	-		-	
214.0(1)	4178→3964	$13^- \rightarrow 12^-$	85(3)	115(5)	0.53(2)	0.97(7)	0.51(3)	0.96(8)
306.8(3)	7417→7109	$19^{(-)} \rightarrow 18^{(-)}$	3.7(4)	8.5(9)			0.71(17)	0.81(19)
312.1(1)	3964→3652	$12^- \rightarrow 11^-$	100(3)	100(3)	0.53(3)	0.99(6)	0.52(4)	0.96(8)
327.0(10)	7142→6815	$16^{(+)} \rightarrow 15^{(+)}$	7.0(5)	12.9(11)	0.44(16)	0.87(23)	0.50(16)	1.51(36)
395.9(1)	3652→3257	$11^- \rightarrow 10$	23.9(11)	18.5(15)		-		-
434.7(2)	5990→5558	$16^{(-)} \rightarrow 15^{(-)}$	6.2(6)	16.6(15)	0.31(9)	1.03(33)	0.47(14)	0.63(11)
543.6(2)	6533→5990	$17^{(-)} \rightarrow 16^{(-)}$	6.2(5)	20.8(14)			0.59(5)	0.83(11)
550.8(2)	6815→6266	$15^{(+)} \rightarrow 14^{(+)}$	2.6(3)	3.1(6)			0.59(22)	
575.4(3)	7109→6533	$18^{(-)} \rightarrow 17^{(-)}$	5.4(6)	19.2(16)			0.39(16)	0.71(10)
646.1(1)	4824→4178	$14^{(-)} \rightarrow 13^-$	37.2(14)	62(3)	0.57(9)	0.85(8)	0.46(6)	0.94(13)
704.6(2)	7846→7142	$17^{(+)} \rightarrow 16^{(+)}$	5.6(5)	12.8(15)			0.72(16)	1.18(31)
734.4(1)	5558→4824	$15^{(-)} \rightarrow 14^{(-)}$	14.5(8)	30.1(18)		0.88(12)	0.58(11)	0.79(10)
780.3(10)	8627→7846	$18^{(+)} \rightarrow 17^{(+)}$	5.0(24)	12.2(17)	0.36(8)		0.93(24)	1.32(21)
802.3(1)	1477→675	$9^+ \rightarrow 8^+$	17.3(24)	12.4(17)	-	0.92(19)		1.01(16)
812.0(10)	3257→2444	$10 \rightarrow 10^+$	0.2(8)	0.2(7)		-		-
944.3(1)	3257→2312	$10 \rightarrow 9^+$	17.6(11)	7.5(16)	-	-	-	-
967.5(3)	2444→1477	$10^+ \rightarrow 9^+$	6.6(9)	4.0(16)	-	1.46(23)	-	
1208.2(1)	3652→2444	$11^- \rightarrow 10^+$	75(3)	51.8(26)	0.54(8)	gate	0.64(7)	gate
1608.4(1)	2312→704	$9^+ \rightarrow 7$	15(2)	10.3(11)	-	-	-	-
1637.7(1)	2312→675	$9^+ \rightarrow 8^+$	8.9(7)	7.9(13)	-	-	-	-
1769.3(1)	2444→675	$10^+ \rightarrow 8^+$	97(4)	51(3)	gate	1.75(8)	gate	1.42(12)
1779.3(2)	3257→1477	$10 \rightarrow 9^+$	11.8(9)	7.6(16)	-	-	-	-
1991.0(2)	6815→4824	$15^{(+)} \rightarrow 14^{(-)}$	5.1(4)	8.3(9)				
2032.6(10)	9142→7109							
2086.8(10)	6266→4178	$14^{(+)} \rightarrow 13^-$	2.2(3)	4.8(9)				
3081.3(10)	9614→6533							

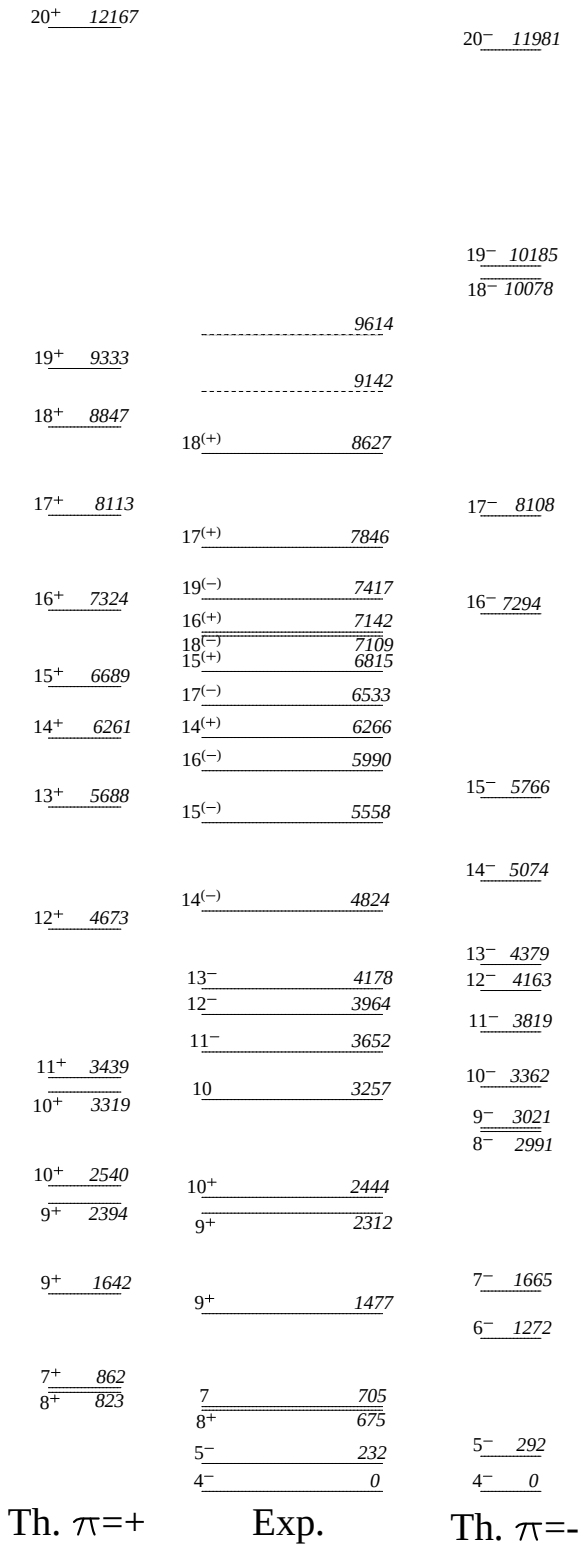

FIG. 5: Experimental level scheme for ^{88}Y constructed from the presented data alongside shell model calculations performed using NuShellX and the jun45 interaction.

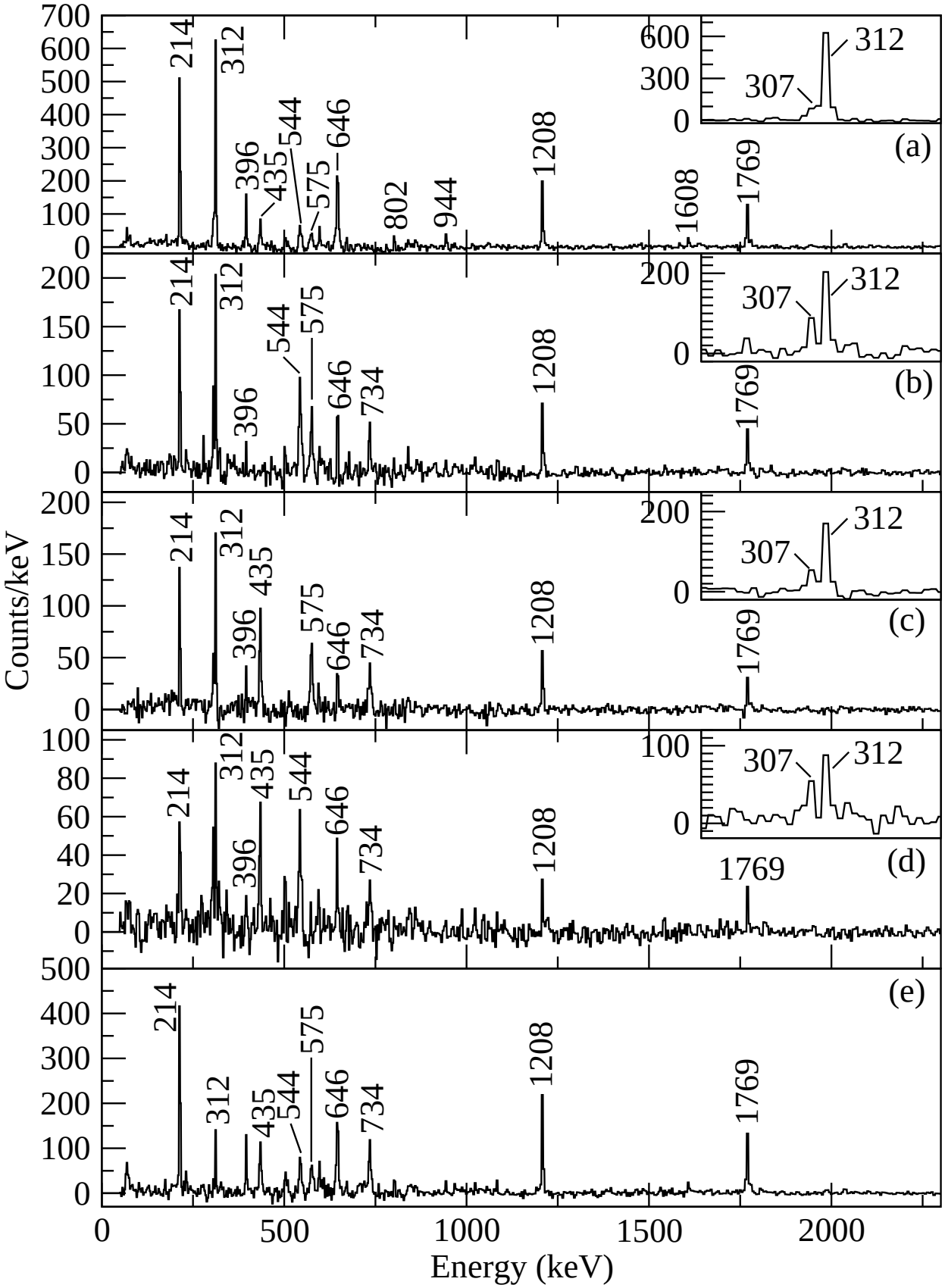

FIG. 6: Evidence for the placement of the transition at the top of the previously reported main cascade from the backed target data. Sum of background subtracted, double gated projections of the symmetrised γ^3 cube with the second energy gates at 214, 312, 646, 1208 and 1769 keV with

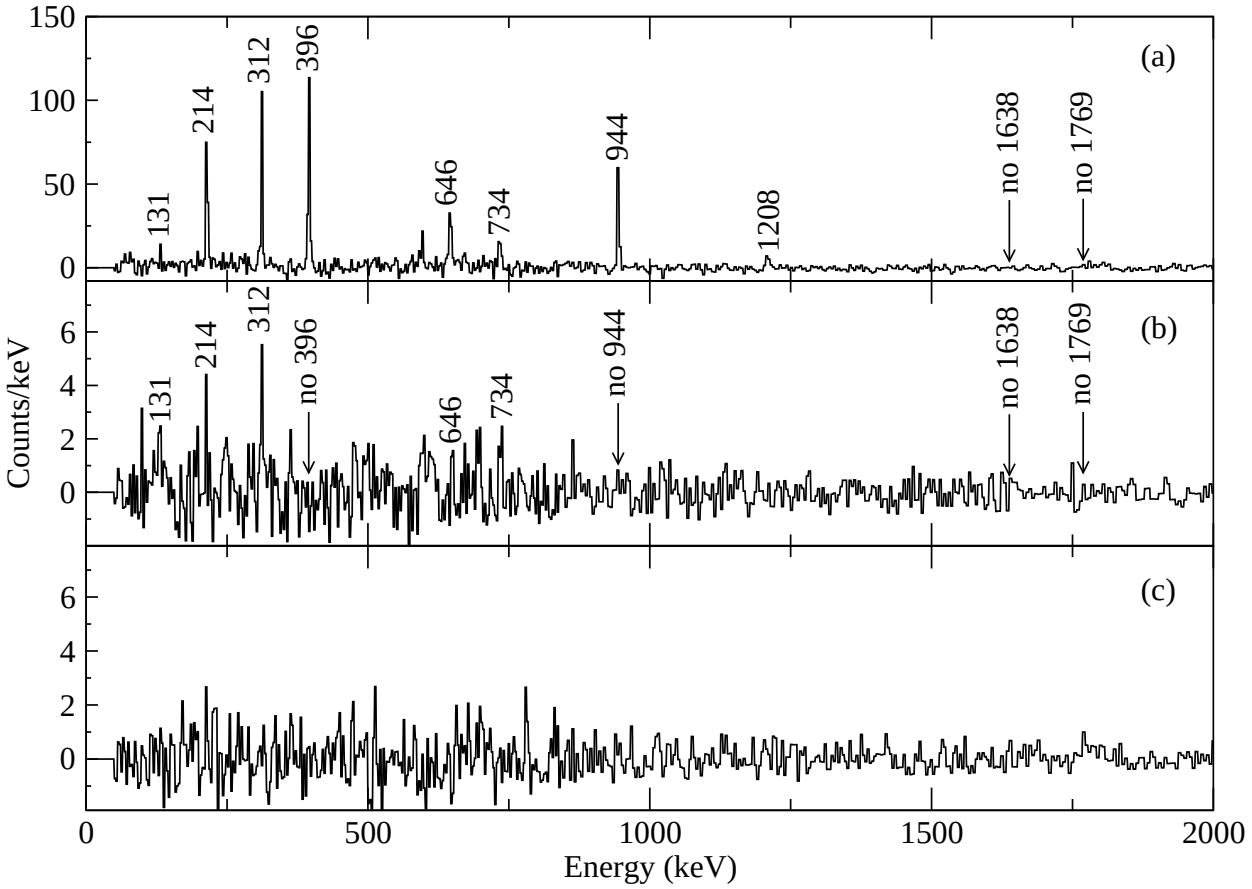

FIG. 7: Projections of double gated symmetrised γ^3 cube for the backed data. (a) Gates on 1608 keV and 312 keV + 214 keV. (b) Gates on 1608 keV and 1208 keV. (c) Gates on 1608 keV and 1769 keV.

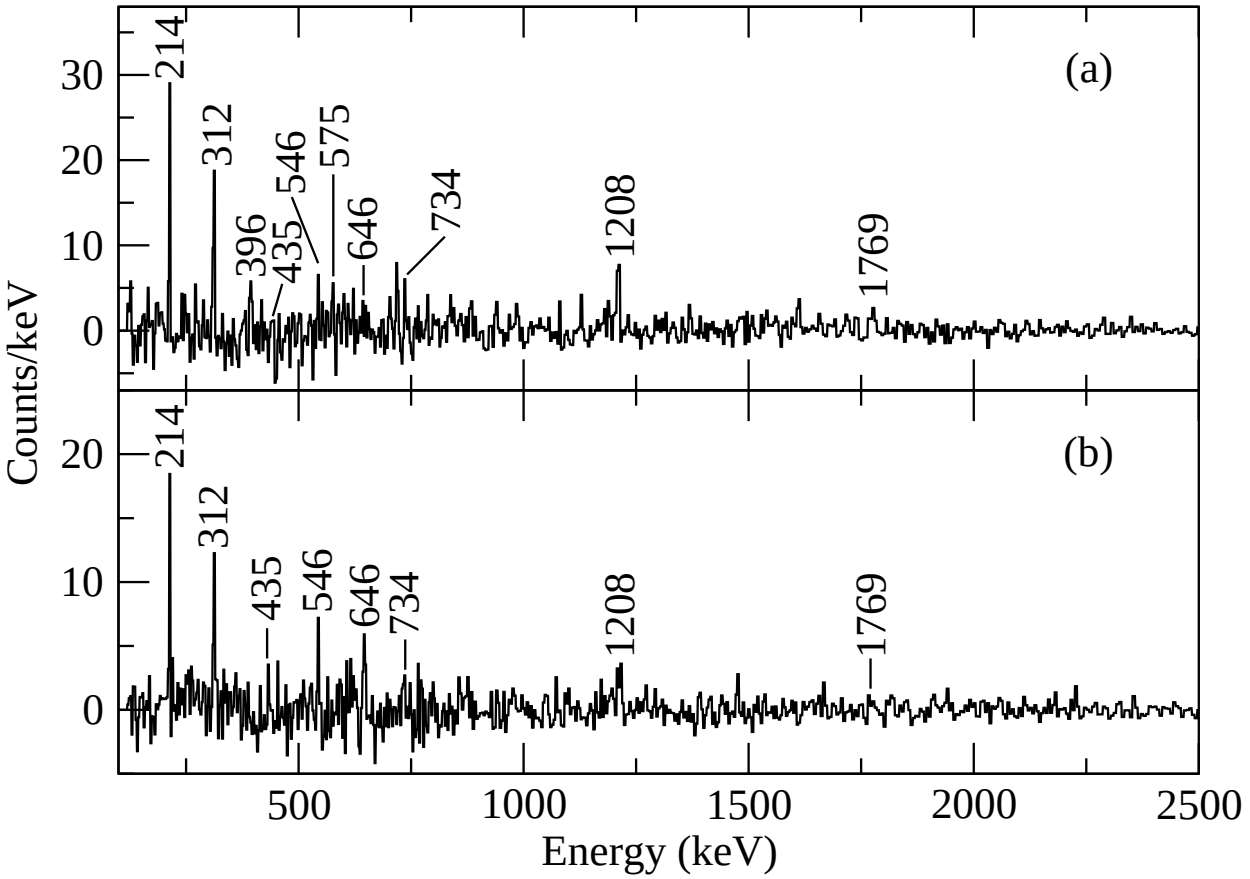

FIG. 8: Projections of background subtracted double gated γ^3 coincidences for the thin target data. (a) Sum of gates between 2033 keV and 214 and 312 keV. (b) Sum of gates between 3081 keV and 214, 312 and 646 keV.

TABLE III: Shell model calculation results for ^{88}Y (see text for details). † Percentage of state wavefunction with this angular momentum coupling. ‡ Percentage of the total state wavefunction with this single-particle configuration.

State		%†	Ang. mom.		%‡	π occupancy			
I^π	E_x (keV)		π	ν		$f_{5/2}$	$p_{3/2}$	$p_{1/2}$	$g_{9/2}$
4^-	0	81	1/2	9/2	50	6	4	1	0
					10	6	2	1	2
5^-	292	88	1/2	9/2	62	6	4	1	0
					11	6	2	1	2
8^+	823	88	9/2	9/2	50	6	4	0	1
					10	6	2	2	1
					10	6	2	0	3
7^+	862	89	9/2	9/2	50	6	4	0	1
					10	6	2	2	1
					10	6	2	0	3
6^-	1272	72	3/2	9/2	37	6	3	2	0
					16	6	3	0	2
9^+	1642	89	9/2	9/2	50	6	4	0	1
					11	6	2	2	1
					10	6	2	0	3
7^-	1665	93	5/2	9/2	38	5	4	2	0
					25	5	4	0	2
					13	5	2	2	2
9_2^+	2394	23	9/2	9/2	6	6	3	1	1
					18	5	4	1	1
		60	11/2	9/2	18	6	3	1	1
					25	5	4	1	1

Continued on next page

TABLE III – continued from previous page

State		%†	Ang. mom.		%‡	π occupancy			
I^π	E_x (keV)		π	ν		$f_{5/2}$	$p_{3/2}$	$p_{1/2}$	$g_{9/2}$
10^+	2540	40	11/2	9/2	11	6	3	1	1
					16	5	4	1	1
		53	13/2	9/2	18	6	3	1	1
					16	5	4	1	1
8^-	2991	78	7/2	9/2	43	6	3	0	2
					10	5	3	1	2
9^-	3021	28	9/2	9/2	16	6	3	0	2
		60	13/2	9/2	44	6	3	0	2
10_2^+	3319	20	11/2	9/2	9	5	4	1	1
		66	13/2	9/2	31	6	3	1	1
					23	5	4	1	1
10^-	3362	85	13/2	9/2	65	6	3	0	2
11^+	3439	95	13/2	9/2	32	6	3	1	1
					27	5	4	1	1
11^-	3819	79	13/2	9/2	50	6	3	0	2
					7	5	4	0	2
					5	6	2	1	2
12^-	4163	15	15/2	9/2	5	6	3	0	2
					6	5	4	0	2
		30	17/2	9/2	7	6	3	0	2
					13	5	4	0	2
		45	19/2	9/2	11	6	3	0	2
					23	5	4	0	2
13^-	4379	40	17/2	9/2	25	5	4	0	2
		37	19/2	9/2	22	5	4	0	2
		19	21/2	9/2	13	5	4	0	2

Continued on next page

TABLE III – continued from previous page

State		%†	Ang. mom.		%‡	π occupancy			
I^π	E_x (keV)		π	ν		$f_{5/2}$	$p_{3/2}$	$p_{1/2}$	$g_{9/2}$
12^+	4673	63	15/2	9/2	24	5	3	2	1
					17	5	3	0	3
		30	17/2	9/2	12	5	3	2	1
14^-	5074	50	19/2	9/2	30	5	4	0	2
		47	21/2	9/2	31	5	4	0	2
13^+	5688	91	17/2	9/2	30	5	3	2	1
					27	5	3	0	3
					7	4	4	0	3
15^-	5766	96	21/2	9/2	62	5	4	0	2
					10	5	2	2	2
					10	5	2	0	4
14^+	6261	58	19/2	9/2	36	5	3	0	3
					9	4	4	0	3
		30	21/2	9/2	15	5	3	0	3
15^+	6689	76	21/2	9/2	49	6	2	0	3
					7	4	4	0	3
		17	23/2	9/2	7	5	3	0	3
16^-	7294	66	23/2	9/2	47	5	3	1	2
		32	25/2	9/2	23	5	3	1	2
16^+	7324	67	23/2	9/2	43	5	3	0	3
					10	4	4	0	3
		22	25/2	9/2	13	5	3	0	3
17^-	8108	98	25/2	9/2	67	5	3	1	2
					8	4	4	1	2

Continued on next page

TABLE III – continued from previous page

State		%†	Ang. mom.		%‡	π occupancy			
I^π	E_x (keV)		π	ν		$f_{5/2}$	$p_{3/2}$	$p_{1/2}$	$g_{9/2}$
17^+	8113	67	25/2	9/2	42	5	3	0	3
					11	4	4	0	3
		23	27/2	9/2	14	5	3	0	3
		9	29/2	9/2	6	5	3	0	3
18^+	8847	68	27/2	9/2	42	5	3	0	3
					10	4	4	0	3
		21	29/2	9/2	19	5	3	0	3
19^+	9333	97	29/2	9/2	59	5	3	0	3
					13	4	4	0	3
					7	5	2	1	3
18^-	10078	63	27/2	9/2	40	5	2	0	4
					7	4	3	0	4
					7	5	1	1	4
		34	29/2	9/2	22	5	2	0	4
19^-	10185	95	29/2	9/2	59	5	2	0	4
					11	4	3	0	4
					9	5	1	1	4
					6	4	2	1	4
20^-	11981	96	31/2	9/2	59	5	2	0	4
					18	4	3	0	4
					6	5	1	1	4
					7	4	2	1	4
20^+	12167	96	31/2	9/2	63	5	2	1	3
					26	4	3	1	3
21^+	12903	100	33/2	9/2	90	4	3	1	3

Continued on next page

TABLE III – continued from previous page

State		%†	Ang. mom.		%‡	π occupancy			
I^π	E_x (keV)		π	ν		$f_{5/2}$	$p_{3/2}$	$p_{1/2}$	$g_{9/2}$
21^-	13357	91	33/2	9/2	44	4	3	0	4
					18	3	4	0	4
					14	4	2	1	4
		8	35/2	9/2	8	4	3	0	4
22^-	13802	99	35/2	9/2	86	4	2	0	5
22^+	15953	98	35/2	9/2	84	4	3	0	4
23^-	16323	100	37/2	9/2	83	4	2	1	4
					15	3	3	1	4
23^+	16948	100	37/2	9/2	83	4	2	0	5
					11	3	3	0	5
24^+	20615	100	39/2	9/2	100	3	2	1	5